



ISSN 0250-3301 CODEN HCKHDV HUANJING KEXUE

中国主要城市土壤重金属累积特征与风险评价彭驰,何亚磊,郭朝晖,肖细元,张严



- 主办 中国科学院生态环境研究中心
- ■出版 斜 孝 出 版 社





2022年1月

第43卷 第1期 Vol.43 No.1

ENVIRONMENTAL SCIENCE

第43卷 第1期 2022年1月15日

目 次

```
无定河流域地表水地下水的水化学特征及控制因素 李书鉴,韩晓,王文辉,李志(220)
白洋淀府河影响区沉积物营养盐和重金属污染特征及风险评价 陈兴宏,李立青,张美一,张伟军,王东升,王洪杰(230)
九龙江口红树林湿地表层沉积物中微塑料赋存特征与重金属的关系 刘倡君,罗专溪,闫钰、林惠荣,胡恭任,于瑞莲(239)
北京市北运河水系底栖动物群落与水环境驱动因子的关系及水生态健康评价 胡小红,左德鹏,刘波,黄振芳,徐宗学(247)
城市河道再生水特征水质因子空间变异机制分析 初全忠,彭柯,苏振华,即琰茗,郭逍宇(256)
苏州景观河道表层沉积物间隙水-上覆水中 DOM 特性分析 李超男,何杰,朱学惠,李学艳(267)
苏州城区雨水管道沉积物典型污染物分布特征 中蓉,盛铭军,姜永波,武宇圣,黄天寅(277)
信号分子强化改性挂膜沸石持续抑制沉积物中氨氮释放 徐金兰,许洋,李修民,国寨,刘成海(285)
三峡水库调度对支流水体叶绿素 a 和环境因子垂向分布的影响 田盼,李亚莉,李莹杰,李虹,王丽婧,宋林旭,纪道斌,赵星星(295)
李家河水库春季分层期 nirS 型反硝化菌群特征分析 张青泽,杨尚业,刘凯文,李程遥,温成成,李伟涛,蔡晓春(306)
岗南水库沉积物好氧反硝化菌群落时空分布特征 张寿泽,张海涵,杨尚业,刘凯文,李程遥,温成成,李伟涛,蔡晓春(306)
它更地区地下水金属元素分布特征及健康风险评价 张紫薇,陈召莹,张甜娜,周石磊,崔建升,罗晓(314)
宁夏地区地下水金属元素分布特征及健康风险评价
张智博,段艳平,沈嘉豪,俞文韬,罗鹏程,涂耀仁,高峻(349)
洞庭湖及入湖河流中 209 种多氯联苯同类物分布特征与风险评估 …… 黄智峰,郑丙辉,尹大强,崔婷婷,赵兴茹(363)
洞庭初及人砌河流中 209 种多氯联苯间实物分布特征与风险评估 更管峰,郑内辉,尹大强,崔婷婷,赵庆如(363)基于流量和溶存浓度的河流水系氧化亚氮释放量估算 "李冰清,胡敏鹏,王铭烽,张育福,吴昊,周佳,吴锴彬,戴之舟,陈丁江(369)三峡库区万州段河流水-气界面 CO。通量支干流对比及影响机制初探 秦宇,欧阳常悦,王雨潇,方鹏(377)功能化凹凸棒吸附材料的制备及其对重金属废水中 Pb² + 的吸附行为 廖晓峰,钟静萍,陈云嫩,邱廷省,任嗣利(387)铁氮共掺杂生物炭对二级水溶解性有机物的吸附特性与长效性评价 吴晨曦,许路,金鑫,石炬,金鹏康(398)沸石悬浮填料生物移动床的亚硝化特性 "邓翠兰,郭露,江晓军,陈振国(409)
雷州半岛南部典型农用地土壤-作物的有机氯农药残留特征和健康风险评价 …… 梁晓晖,解启来,郑芊,杨北辰,叶金明,唐成金(500)
重金属含量对城市土壤真菌群落结构的影响 …………………………………………郭大陆,张建,申思,余子洁,杨军顺,罗红燕(510)
长期施肥对黄土高原梯田土壤养分特征和微生物资源限制的影响 …… 吴春晓,高小峰,闫本帅,梁彩群,陈佳瑞,王国梁,刘国彬(521)
土地利用变化后不同种植年限香榧土壤微生物群落的组成及多样性 …… 姜霓雯, 梁辰飞, 张勇, 蒋仲龙, 董佳琦, 吴家森, 傅伟军 (530)
化肥和有机肥配施生物炭对土壤磷酸酶活性和微生物群落的影响 ····· 杨文娜, 余泺, 罗东海, 熊子怡, 王蓥燕, 徐曼, 王子芳, 高明(540)秦岭中段撂荒地植被恢复过程中土壤微生物代谢特征 ··········· 薛悦, 康海斌, 杨航, 冰德叶, 晁志, 张凯, 王得祥(550)全生物降解地膜原料颗粒对土壤性质、小麦生长和养分吸收转运的影响
《环境科学》征订启事(73) 《环境科学》征稿简则(209) 信息(229, 266, 338)
```



中国东部冷锋推进中的 PM2.5 三维结构变化特征

牟南南, 朱彬*, 卢文

(南京信息工程大学气象灾害预报预警与评估协同创新中心,气象灾害教育部重点实验室,国家综合气象观测专项试验外场,南京 210044)

摘要:利用观测资料和中尺度天气-化学模式(WRF-Chem)对一次冷锋南下天气过程导致的我国东部大范围空气污染开展研究,强调了冷锋过境前后的边界层结构及其对 PM_{2.5}三维结构和变化的影响.观测发现,地面重污染区域位于冷锋前部均压场或等压线稀疏区域,在冷锋由北向南快速移动过程中,途经各站点 PM_{2.5}浓度峰值伴随锋前而至. WRF-Chem 模式可以较好地模拟中国东部地面和高空气象要素以及 PM_{2.5}浓度的时空变化.模拟结果表明,处于该移动冷锋天气系统相同位置的沿途各站点的边界层结构以及 PM_{2.5}垂直廓线表现出相似的特征.即:当冷锋开始人侵时,锋前污染物从地面被抬升到高空,PM_{2.5}浓度的增加和高空风速的增大导致高空 PM_{2.5}通量增大,且 PM_{2.5}浓度高值区随着高度升高向暖气团一侧倾斜.夜间冷锋过境引发边界层内对流性不稳定增加,边界层高度可达 1 km 以上,打破了边界层昼夜演变特征.本研究表明,垂直观测和精细模拟的结合可以有效地解释天气过程对空气污染的输送、分布和演变的影响,并为区域空气污染归因和治理提供精确指导.

关键词:数值模拟;空气污染;边界层结构;气象要素;PM,。三维结构

中图分类号: X513 文献标识码: A 文章编号: 0250-3301(2022)01-0085-08 DOI: 10.13227/j. hjkx. 202103116

Three-dimensional Structure Variation of $PM_{2.5}$ During Cold Front Advance in Eastern China

MOU Nan-nan, ZHU Bin*, LU Wen

(Outfield of National Comprehensive Meteorological Observation Special Experiment, Key Laboratory of Meteorological Disaster, Ministry of Education, Collaborative Innovation Center on Forecast and Evaluation of Meteorological Disasters, Nanjing University of Information Science and Technology, Nanjing 210044, China)

Abstract: Based on observational data and the WRF-Ghem model, this study analyzed the large-scale air pollution in eastern China, which was caused by the weather process of a cold front moving southward, emphasizing the vertical structure of the boundary layer and the influence on the three-dimensional structure of PM_{2.5}. Our observations revealed that the heavy pollution near the surface was located at sparse or equal isobar in front of the cold front. During the process of the weather system moving in, the timing of the maximum PM_{2.5} concentration at each station from north to south was delayed. The results show that the WRF-Chem model can better capture the spatial and temporal variations of surface and upper air meteorological elements and PM_{2.5} concentrations over eastern China. The simulation results show that the boundary layer structure and the vertical profile of PM_{2.5} at the same location of the mobile weather system showed similar characteristics. When the invasion takes place in a cold front, the pollutants in front of the cold front are rapidly lifted from the ground to a high altitude. The growth in PM_{2.5} concentration and the increasing wind speed at high altitudes lead to the upward trend in PM_{2.5} flux. As the altitude increases, the high-value area of PM_{2.5} concentration tilts towards the warm air mass. The transit of the cold front at night led to more unstable convection within the boundary layer; the height of the boundary layer increased from north to south, reaching over 1 km, breaking the rules characteristic of the diurnal evolution of the boundary layer. The results indicate that the combination of vertical observations and elaborate simulation can effectively explain the impact of synoptic processes on the transport, distribution, and evolution of air pollution and provide precise pollution-control directives.

Key words: numerical simulation; air pollution; boundary layer structure; meteorological elements; three-dimensional structure of PM2 5

近年来,气溶胶及其前体物的排放加剧了中国的空气污染.特别是在人口密度高且工业化进程快的地区,空气动力直径 < 2.5 μm 的气溶胶细粒子 (PM_{2.5})是我国主要的大气污染物^[1,2].高浓度的颗粒物加剧了雾-霾事件的发生^[3],不仅对城市环境、交通安全造成显著影响,也会引起肺炎、支气管炎和心血管等疾病,严重威胁人类健康^[4-6]. 2013 年以来由于大气污染防治行动计划的实施,颗粒物浓度持续下降^[7],但颗粒物污染事件仍然频发,尤其是在秋冬季.

有研究表明,大气扩散和传输使大气污染物重新分布,而天气系统对于大气扩散和传输条件有重要影响,它提供了区域空气污染变化的主要驱动力^[8].局地大气污染物的积聚、清除以及长距离传

输^[9],在不同天气形势下有显著的差异^[10].一般来说,近地面稳定的反气旋环流有利于空气污染的形成,而气旋系统相对不会造成严重的空气污染^[11].冬季由于有西伯利亚冷高压活跃并南下,冷锋可作为污染物的载体把北方上游的污染物传输至下游使下游地区空气质量恶化^[12].在一定的天气形势下,气温、风速及风向等气象要素水平和垂直分布的不同直接影响着大气边界层的垂直结构以及气溶胶的水平和垂直分布特征.有研究发现,地面高相对湿度、低风速和稳定层结大气抑制了大气污染物的迁

收稿日期: 2021-03-12; 修订日期: 2021-06-08

基金项目: 国家自然科学基金项目(92044302, 42021004)

作者简介: 牟南南(1995~),女,硕士研究生,主要研究方向为大气 污染与大气环境,E-mail;nannan_m@163.com

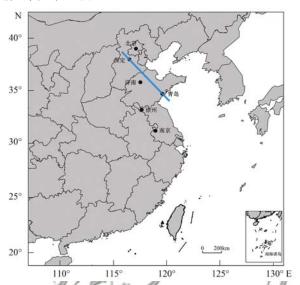
* 通信作者,E-mail;binzhu@nuist.edu.cn

移和扩散,强逆温层和较低的混合层高度有助于污 染物累积[13~15]. 气溶胶的直接效应使边界层低层减 温和高层增温,从而大气层结更稳定,进而使得边界 层的高度更低和边界层内的湍流扰动更弱,这造成了 对 PM, 5浓度聚积的正反馈[16,17]. 目前我国已开展了 一些应用不同空气质量模型对大气污染物区域传输 的研究,蒋永成[18] 通过 WRF-Chem 模式对海西区 2013年1月霾污染过程进行模拟研究,阐明了大气污 染物的区域输送对低污染源区空气质量的影响很大: Yu 等[19]的研究使用 FLEXPART-WRF 模式对长江中 游地区强北风、无逆温即大气层结不稳定条件下的 PM,5污染事件进行模拟,发现 PM,5的区域输送对重 度污染 PM2.5浓度的贡献率超过65%. 杨旭等[20]结合 无人机探空和数值模拟对天津一次重污染事件研究, 发现区域污染物的输送高度主要在边界层顶部和逆 温层以上的大风速层处,且输送和边界层反馈作用对 雾-霾天气的影响是相互的[21].

前人主要针对近地面 PM_{2.5}污染以及区域输送开展了很多观测和模拟分析研究,但对垂直方向 PM_{2.5}和边界层结构相结合的分析研究还较少.对空气污染事件中,天气形势移动和变化下的 PM_{2.5}的三维结构和演化还了解甚少.本文利用 WRF-Chem 模式针对2019 年 1 月 14~15 日我国东部受冷空气影响发生的一次大范围 PM_{2.5}污染事件开展模拟研究,结合同期在南京开展的一次边界层气象-大气污染的垂直观测数据,分析冷锋移动的天气形势下,边界层结构的变化及其对 PM_{2.5}浓度三维分布和变化的影响,以期为区域空气污染成因和评估提供科学指导.

1 模式设置与验证

本次研究采用中尺度天气-化学模式(WRF-Chem) 3.4 版本,模拟前用 MICAPS 气象观测资料对 气象场进行了同化,同化采用的方法为牛顿张弛逼 近法(nudging),它在预报方程中额外增加一个松弛 项,表示预报与观测值之差,从而使模拟值向观测值 逼近,使用 MICAPS 地面数据作为数据源,同化的变 量包括温度、比湿和 UV 风速[22,23],其中气象场使 用 ECMWF 0.25°×0.25°再分析资料.模拟区域包 括中国中东部和周边的海洋(图1),中心经纬度为 119.0°E、31.5°N,包含99×99个网格,水平分辨率 为27 km. 模式层顶设置为50 hPa 高度处,自地表到 模式层顶共分38层,2km以下约为12层.模式的 模拟时间为 2019 年 1 月 1 日 00:00 至 1 月 23 日 00:00(北京时),将模拟前48 h 设置为 spin-up 的时 间. 边界层方案使用 Mellor-Yamada-Janjic (Eta) TKE[24]方案,该方案用边界层和自由大气中的湍流 参数化过程代替 Mellor-Yamada 的 2.5 阶湍流闭合模型. 排放源使用清华大学提供的 MEIC(2016)源清单(http://www. meicmodel. org/),分辨率为0.25°×0.25°,使用全球化学模式 MOZART-4^[25]提供化学初始条件以及化学边界条件,生物质源则使用 MEGAN 模式在线生成^[26]. 本次模拟中其他参数化方案如表 1 所示.



北京、济南、青岛和南京为模式评估所选站点; 蓝色实线表示后续论述的垂直界面方向

图 1 WRF-Chem 模式模拟区域 Fig. 1 WRF-Chem Model domains

表 1 WRF-Chem 模式参数设置

Table 1 Model parameter setting

	1 8
物理过程	参数化方案
微物理过程	Lin
长/短波辐射	RRTMG
陆面过程	Noah Land Surface Model
积云对流	Grell-Devenyi ensemble scheme
干沉降过程	Wesley
光解率	Fast-J

为了检验模式对 PM_{2.5}和气象要素的模拟性能,将模拟区域内 4 个代表站点(北京、济南、青岛和南京)的 PM_{2.5}浓度、温度、风速和风向的模拟以及观测结果进行了对比,其中 PM_{2.5}浓度观测值为中国环保部提供的逐小时数据,地面气象要素观测值来自 MICAPS 提供的 3 h 一次地面全要素填图数据.图 2 为 PM_{2.5}浓度以及各个气象要素模拟值与观测值的时间序列对比. 2019 年 1 月 12 ~ 26 日,在南京市浦口区设置观测点(32.2°N,118.7°E)开展外场地面和边界层气象与大气污染垂直观测实验.图 3 为 1 月 15 日南京 PM_{2.5}污染期间,PM_{2.5}浓度、风矢量和温度垂直分布的观测和模拟对比.可以看出该模型再现了模拟时间段内各气象要素和 PM_{2.5}浓度的数值大小和变化特征,其中所有站点温度模拟得

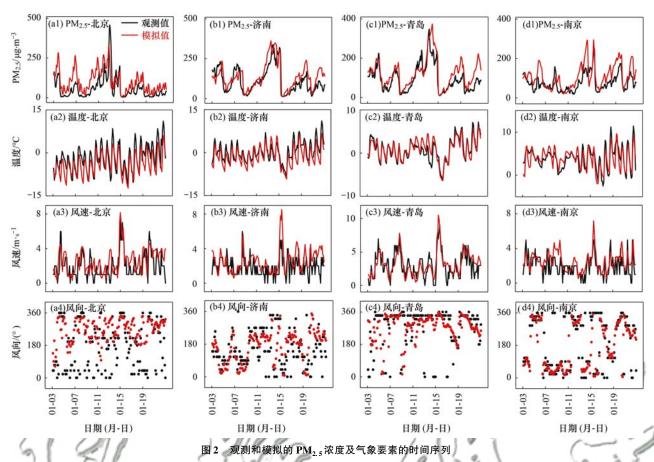


Fig. 2 Time series of observed and simulated PM2 5 mass concentration and meteorological elements

最好. 尽管这期间风速变化较为剧烈,但总体上模拟的结果能有效地再现风速的日变化特征,大部分时期风向的观测值和模拟值也有较好的一致性. 4 个站点 PM_{2.5}浓度的观测值与模拟值的一致性较好,模

拟值略偏高. 垂直方向上(图 3), 1 月 15 日白天南京发生污染期间 PM_{2.5}浓度和温度的模拟值和观测值的变化趋势相似,可以有效再现 PM_{2.5}浓度以及气象要素垂直方向的变化特征.

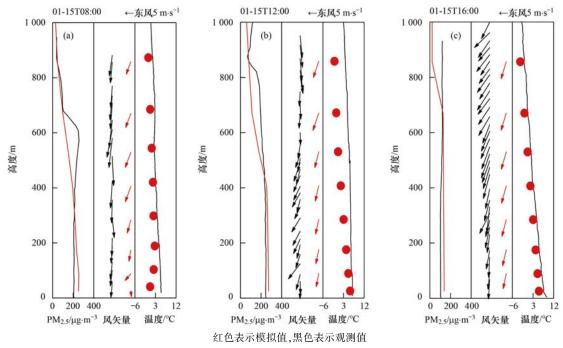


图 3 南京观测和模拟的 PM_{2.5} 浓度、风矢量和温度的垂直分布

Fig. 3 Vertical distribution of observed and simulated $PM_{2.5}$ mass concentration, wind, and temperature

为了进一步验证模拟效果,运用 Pearson 相关系数(R)、一致性指数(IOA)、总偏差(GE)、平均分数偏差(MFB)、平均分数误差(MFE)和均方根误差(RMSE)这几个统计特征量对模拟结果的准确性进行验证(表 2). 风向的 IOA 指数(IOAwdir),是按照Kwok 等[27]的研究方法,根据风的矢量特性单独计算的. 所用统计量公式如下:

88

$$R = \frac{\operatorname{Cov}(x, y)}{\sqrt{D(x)} \cdot \sqrt{D(y)}} \tag{1}$$

IOA = 1 -
$$\frac{\sum_{i=1}^{N} (M_i - O_i)^2}{\sum_{i=1}^{N} (|M_i - \overline{M}| + |Q_i - \overline{O}|)^2}$$
 (2)

$$GE = \frac{1}{N} \sum_{i=1}^{N} |M_i - O_i|$$
 (3)

MFB =
$$\frac{1}{N} \sum_{i=1}^{N} \frac{(M_i - O_i)}{(O_i - M_i/2)}$$
 (4)

MFE =
$$\frac{1}{N} \sum_{i=1}^{N} \frac{|M_i - O_i|}{(O_i - M_i/2)}$$
 (5)

RMSE =
$$\left[\frac{1}{N} \sum_{i=1}^{N} (M_i - O_i)^2\right]^{1/2}$$
 (6)

式中, M_i 为模式模拟值, O_i 为观测值.

所有评估站点的 $PM_{2.5}$ 、温度和湿度的相关系数均大于 0.67,并达到显著性水平 (α = 0.01). $PM_{2.5}$ 、温度、风速、风向和湿度的一致性指数分别大于 0.7、0.83、0.61、0.78 和 0.7,各参数的相关性和一致性指数都较高. 4 个站点 $PM_{2.5}$ 的 MFB 范围为 $0.2 \sim 0.6$,MFE 在 $0.26 \sim 0.65$ 之间,它们都符合 Boylan 等 $[^{28}]$ 的研究提出的标准: 当 MFB 在 ± 0.6 以内,MFE 在 0.75 以下时,模型性能良好. 所有站点的风速的 RMSE 均符合阈值 (≤ 2.0),虽然风向的相关系数较低,但 IOA 均在 0.78 以上,说明风速、风向的模拟值和观测值在变化趋势上有较好吻合. 其中温度的模拟效果最好,4 个站点温度的 R 和 IOA 均大于 0.79,除北京站外其它 3 个站点的 GE

都符合标准阈值(≤2.0).整体上认为本次模拟效果良好,其中温度、湿度的模拟效果优于风速风向,本次模拟结果可以较好地重现我国东部地区地面气象要素和 PM_{2.5}的时空分布特征.

表 2 PM_{2.5}浓度和气象要素(温度、风速、 风向和湿度)的统计检验结果

Table 2 Statistical test results of PM_{2.5} mass concentration and meteorological elements (temperature, wind speed,

wind direction, and humidity)				
统计特征量	北京	济南	青岛	南京
R	0. 67	0.80	0. 85	0.71
IOA	0.70	0.87	0.88	0.71
MFB	0.60	0.20	0. 23	0.24
MFE	0.65	0. 29	0. 26	0.33
R	0.81	0.86	0.88	0. 79
IOA	0.83	0.87	0.94	0.88
GE	2. 68	1.89	0.88	1.3
RMSE	3. 35	2. 27	1. 24	1.61
R	0.58	0.51	0.78	0. 59
IOA	0. 72	0.61	0.87	0.69
GE	1. 14	1.05	0.97	0.88
RMSE	1.46	1.38	1. 23	1. 13
R	0. 19	0.48	0.16	0. 57
IOA	0. 78	0.87	0.88	0.93
RMSE	155. 96	92.44	119. 53	122. 21
// R	0. 67	0.83	0. 78	0.85
IOA	0. 7	0.88	0. 85	0.88
MFB	0. 24	0. 1	0.02	-0.04
MFE	0.31	0. 17	0. 11	0.08
	统计特征量 R IOA MFB MFE R IOA GE RMSE R IOA GE RMSE R IOA GE RMSE R IOA MFB	统计特征量 北京 R 0.67 IOA 0.70 MFB 0.60 MFE 0.65 R 0.81 IOA 0.83 GE 2.68 RMSE 3.35 R 0.58 IOA 0.72 GE 1.14 RMSE 1.46 R 0.19 IOA 0.78 RMSE 155.96 R 0.67 IOA 0.7 MFB 0.24	统计特征量 北京 济南 R 0.67 0.80 IOA 0.70 0.87 MFB 0.60 0.20 MFE 0.65 0.29 R 0.81 0.86 IOA 0.83 0.87 GE 2.68 1.89 RMSE 3.35 2.27 R 0.58 0.51 IOA 0.72 0.61 GE 1.14 1.05 RMSE 1.46 1.38 R 0.19 0.48 IOA 0.78 0.87 RMSE 155.96 92.44 R 0.67 0.83 IOA 0.7 0.88 MFB 0.24 0.1	统计特征量 北京 済南 青岛 R 0.67 0.80 0.85 IOA 0.70 0.87 0.88 MFB 0.60 0.20 0.23 MFE 0.65 0.29 0.26 R 0.81 0.86 0.88 IOA 0.83 0.87 0.94 GE 2.68 1.89 0.88 RMSE 3.35 2.27 1.24 R 0.58 0.51 0.78 IOA 0.72 0.61 0.87 GE 1.14 1.05 0.97 RMSE 1.46 1.38 1.23 R 0.19 0.48 0.16 IOA 0.78 0.87 0.88 RMSE 155.96 92.44 119.53 R 0.67 0.83 0.78 IOA 0.7 0.88 0.85 MFB 0.24 0.1 0.02

2 结果与讨论

2.1 天气形势与空气污染概况

取 2019 年 1 月 9~17 日时间段内的北京、保定、济南、青岛、徐州和南京这 6 个站点(图 1)根据经纬度由北向南作 PM_{2.5}浓度和风矢量的时空分布,由图 4 可见,1 月 11~14 日我国华北地区出现PM_{2.5}持续区域性重度污染;1 月 14 日 17:00 至 1 月 16 日 02:00,PM_{2.5}浓度高值区随时间自北向南快速推移,且高值区对应强偏北风,PM_{2.5}峰值浓度均大于 150 µg·m⁻³,污染强度为重度-严重污染.由北到南浓度峰值滞后时间约为 33 h,表现出这股强烈

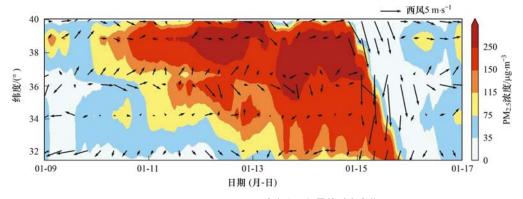


图 4 1月9~17日 PM_{2.5}浓度和风矢量的时空变化

Fig. 4 Temporal and spatial variation in PM_{2.5} concentrations and wind vectors from January 9 to 17

的偏北气流将污染气团从华北地区快速吹向长三角地区的形态;之后,随着强冷空气不断南下,PM_{2.5}由北向南得到了有效地清除.

结合地面天气[图 5(a)]和模拟的 PM_{2.5}浓度水平分布[图 6(b)~6(d)],1月14日17:00高压中心位于蒙新高地上,高压前部的冷锋刚刚到达华北平原北部,华北北部地面等压线密集;而华北中南部地区受高压底前部的均压场控制,地面等压线稀疏,地面风速较小,大气扩散能力较差.此时河北南

部和山东西部的空气污染较为严重, $PM_{2.5}$ 浓度最高超过 300 μ g·m⁻³. 此后高压中心增强,在高空槽后西北气流的引导下向东南方向移动,伴随冷空气东移南下,冷锋进一步向南推移; 1 月 15 日 08:00[图 5(b)],河北南部和山东大部受锋后偏北大风影响,大气扩散条件转好, $PM_{2.5}$ 浓度显著降低,而 $PM_{2.5}$ 高值区随冷空气由北向南移动. 冷锋主体人海后冷锋残留继续将污染物向南推移,直至 1 月 16 日02:00,污染带被输送至长江中游地区.

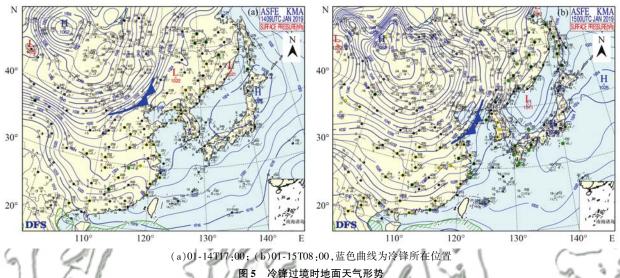
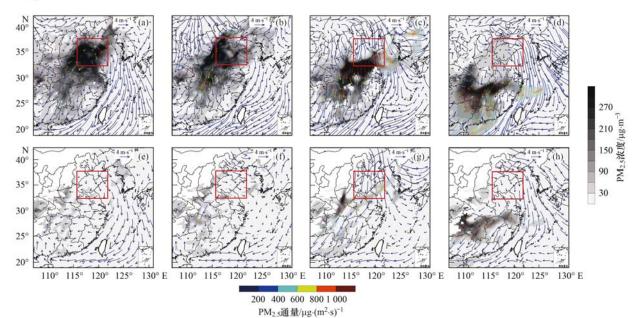


Fig. 5 Surface weather patterns as the cold front passes through

2.2 天气系统移动中边界层结构的变化及其对 PM_{2.5}分布的影响

为了研究冷锋前后的 PM_{2.5}在地面和高空分布

特征,将地面和 1 km 高度处的 $PM_{2.5}$ 浓度分布以及 $PM_{2.5}$ 通量进行对比研究. 由图 6(a) 和 6(e) 可见, 1 月 13 日 23:00 的静稳污染时华北大部地区地面污



(a)~(d)地面,(e)~(h)1km高度; (a)和(e) 01-13T23:00,(b)和(f) 01-14T 17:00,(c)和(g) 01-15T 08:00, (d)和(h)01-16T 02:00; 箭头:风矢量; 红框:华北地区; 箭头颜色:PM25通量

图 6 地面和 1 km 高度 PM_{2.5}浓度、PM_{2.5}通量和风矢量分布

Fig. 6 $PM_{2.5}$ mass concentrations, $PM_{2.5}$ fluxes, and wind vectors at ground level and a 1 km altitude

染较为严重,地面和 1 km 高度处平均 $PM_{2.5}$ 浓度分别为 209. 2 μ g·m⁻³和 17. 3 μ g·m⁻³,高低空浓度差别很大,这与静稳阶段 $PM_{2.5}$ 大部分被压在很低的边界层之下有关. 当冷锋于 1 月 14 日 17:00 刚刚到达华北平原北部边缘时[图 6(b)和 6(f)],地面 $PM_{2.5}$ 尚未受到冷锋的影响,但在 1 km 高度上华北北部开始出现 $PM_{2.5}$ 高值带,在地面和 1 km 处的 $PM_{2.5}$ 平均通量分别为 406. 5 μ g·(m²·s)⁻¹和 230. 10 μ g·(m²·s)⁻¹. 随着冷锋继续向南推移,1 月 15 日 08:00 冷锋到达山东南部,1 km 高度污染带更加明显[图 6(c)和 6(g)]. 由于高空风力较强,高空 $PM_{2.5}$ 高值带先于地面到达,在地面和 1 km 高度处 $PM_{2.5}$ 平均通量分别为 656. 26 μ g·(m²·s)⁻¹和 354. 36 μ g·(m²·s)⁻¹. 在 1 月 16 日 02:00 冷锋继续将污染物推移到长江中游地区[图 6(d)和 6(h)],

高空 $PM_{2.5}$ 通量在锋区进一步加强,达到 430.87 $\mu g \cdot (m^2 \cdot s)^{-1}$,对应的地面通量减小到 513.98 $\mu g \cdot (m^2 \cdot s)^{-1}$.随着冷锋向南侵入,锋面运动将空气污染物从地面快速抬升到高空,高空风速大于地表从而增加了高空 $PM_{2.5}$ 通量逐渐增强^[13].

观测研究发现,在天气系统移动中,位于天气系统相同部位站点的边界层结构具有共同的特征^[29,30].为了更好地判断天气系统途经的各地边界层结构是否发生相似的变化,使用模拟结果分析本次冷空气南下过程中由北至南各站点边界层和PM_{2.5}浓度垂直结构特征.针对冷锋主体扫过区域,选取保定、济南和青岛这3个站点,分析地面锋线到达该三站点之前的温度、风矢量和PM_{2.5}浓度的垂直廓线,并与静稳污染时作对比(图7).

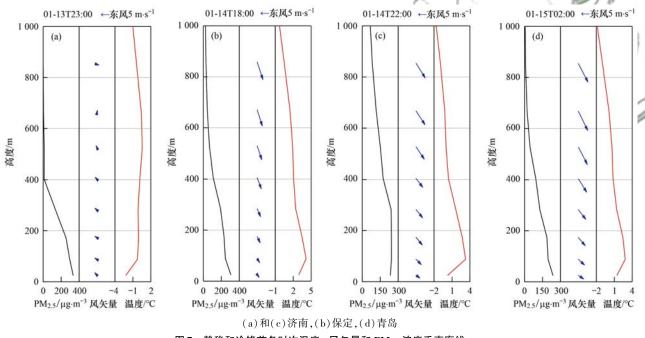


图 7 静稳和冷锋前各时次温度、风矢量和 PM_{2.5}浓度垂直廓线

Fig. 7 Vertical profiles of temperature, wind and $PM_{2.5}$ mass concentration at each time of static stability and before the cold front

静稳污染时刻的 1 月 13 日 23:00 济南站 200 m 以下和 250 ~ 550 m 高度均有逆温层出现,1 km 以下风速均小于 2 m·s⁻¹,整层大气层结稳定,PM_{2.5}浓度随高度升高明显减少.1 月 14 日 18:00,保定地面 PM_{2.5}浓度 > 200 μ g·m⁻³,为重度污染,此时保定处于高压底前部的等压线稀疏区域,在 100 m 以下有贴地逆温存在,逆温强度 1. 2°C·(100 m)⁻¹,400 ~ 530 m 出现弱逆温层,大气层结很稳定.对应 100 m ~ 200 m 高度处于同一层结中,该处 PM_{2.5}浓度变化不大. 从风矢量来看,200 m 以下偏西风,风速 < 2 m·s⁻¹,200 m 以上开始转为北到西北风.1 月 14 日 22:00,济南在 100 m 以下仍有贴地逆温,强度

4.8 ℃·(100 m) $^{-1}$, 430 m ~ 600 m 温度递减率极小,近乎中性层结,整层风都变为西北风, 100 m ~ 300 m 处 $PM_{2.5}$ 浓度保持稳定. 1 月 15 日 02:00,青岛站与济南站温度和风廓线特征相似, $PM_{2.5}$ 垂直廓线与保定站亦类似.

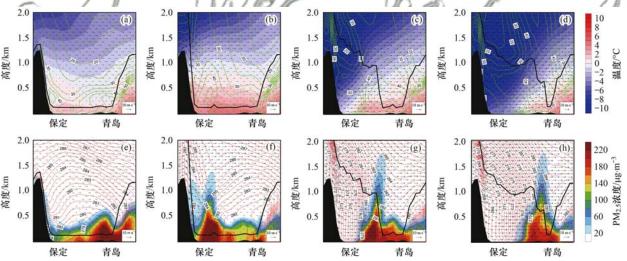
比较图 6(b)、6(c)和 6(d)和前段分析可见,当天气系统移动时处于同一天气系统相同位置的站点边界层结构具有相似性,边界层特征随天气系统的移动而做类似的改变.与发生静稳污染时相比[图 6(a)],冷锋移动过程中整层风速较大,高空为北-西北大风,贴地逆温层顶至边界层上部 PM_{2.5}浓度随高度变化不明显.

2.3 冷锋推进中 PM_{2.5}垂直结构和变化

沿冷锋主体移动方向(保定-青岛)作气象要素 (温度、湿度和风矢量)以及 $PM_{2.5}$ 浓度和假相当位 温 θ_{se} 的垂直剖面可见(图 8), 1 月 14 日 17:00 由于日落后热力作用减弱使边界层内湍流变弱[图 8 (b)],边界层高度仅为 130 m,不利于 $PM_{2.5}$ 的扩散.此后由于冷锋开始过境,冷气团将暖气团抬升.尽管处于夜间, $\partial\theta_{se}/\partial z$ 却由 > 0 转为 < 0 [图 8 (g)],即对流不稳定性增加,导致边界层高度由北向南依次得以抬升,使大气边界层昼夜演变特征基本消失.

1月13日23:00地面为静稳污染时[图8(a)和8(e)], $PM_{2.5}$ 浓度在600m左右可到达60μg·m⁻³,温度递减率为-3.5℃·km⁻¹.1月14日凌晨保定附近有弱偏南风,遇太行山脉的阻挡导致气流略微地上升,使污染物在山前堆积并抬升,1月14日17:00保定垂直方向 $PM_{2.5}$ 达到1.3km高度[图8(b)和8(f)],远大于边界层200m高度;此时冷锋到达华北北部边缘,低层风速小于2m·s⁻¹,高空风速较静稳期明显增大,3km以下 $\theta_{sc}/\partial z > 0$,绝对稳定的大气层结不利于污染物的扩散.冷锋继续

南移,1月14日23:00冷气团控制保定地区「图8 (c)和8(g)],整层风速增大,水平方向上 θω等值 线密集(冷平流); 而垂直方向 100~1000 m处 $\partial\theta_{sc}/\partial z<0$ 为对流不稳定层结,边界层高度抬升至 1.3 km,有利于污染物浓度垂直和水平方向的扩 散,保定空气质量好转.冷锋过境带来冷而干的空 气使河北南部相对湿度减小至 15%~20%. 此时, 山东大部地区 PM25在水平和垂直方向上仍较高, 垂直最高可到达 1.7 km 左右. 1 月 15 日 02:00 山 东大部受冷气团抬升影响「图 8(d)和 8(h)],边 界层至1 km 以上,只有山东东部(青岛上空)冷锋 还未到达, 边界层还很低(~250 m). 由 [图 8(a) ~6(d)]可见,PM,5随冷锋前部推移,由于地表摩 擦作用,高层风速大于地面,导致高空 PM,5传输 较近地面快,PM,5浓度随着高度升高向暖气团一 侧倾斜. 进一步说明随着冷锋向南入侵, PM, ,被向 上抬升,锋面活动能够将空气污染物从地面输送 到高空,导致1 km 以上高空 PM25浓度和 PM25通 量增加.相比于陆地,由于海水比热容大,海上边 界层高度 ·直稳定维持在 1 km 以上.



(a)和(e) 01-13T23:00,(b)和(f)01-14T 17:00,(c)和(g) 01-14T 23:00,(d)和(h)01-15T 02:00; 黑色实线:边界层高度,箭头:风矢量; (a) ~ (d)绿色虚线表示相对湿度; (e) ~ (f)红色虚线表示假相当位温 θ_{se}

Fig. 8 Vertical cross sections of temperature, relative humidity, PM2 5 concentration, and equivalent temperature

图 8 温度、湿度、 $\mathrm{PM}_{2.5}$ 浓度和假相当位温 $heta_{\mathrm{se}}$ 垂直截面

3 结论

- (1)观测发现,地面重污染区域位于冷锋前部 均压场或等压线稀疏区域. 在冷锋由北至南快速移 动过程中,途经各站点 PM_{2.5}浓度峰值伴随锋前而 至. WRF-Chem 模式可以较好地模拟中国东部地面 和高空气象要素以及 PM_{2.5}浓度的时空变化.
- (2)模拟结果表明,处于该移动冷锋天气系统相同位置的沿途各站点的边界层结构以及 PM_{2.5}垂直廓线表现出相似的特征,贴地逆温层顶至边界层
- 上部的 PM_{2.5}浓度随高度不明显. 当冷锋开始入侵时,锋前污染物从地面被抬升到高空,PM_{2.5}浓度的增加和高空风速的增大导致高空 PM_{2.5}通量增大,且 PM_{2.5}浓度高值区随着高度升高向暖气团一侧倾斜.
- (3)夜间冷锋过境引发边界层内对流性不稳定增加,边界层高度由北到南依次得以抬升,可达 1 km 以上,打破了边界层昼夜演变特征.

参考文献:

[1] Wang J D, Zhao B, Wang S X, et al. Particulate matter pollution over China and the effects of control policies [J].

- Science of the Total Environment, 2017, 584-585; 426-447.
- [2] Han R, Wang S X, Shen W H, et al. Spatial and temporal variation of haze in China from 1961 to 2012 [J]. Journal of Environmental Sciences, 2016, 46: 134-146.
- [3] Zhu Q Z, Liu Y Z, Jia R, et al. A numerical simulation study on the impact of smoke aerosols from Russian forest fires on the air pollution over Asia[J]. Atmospheric Environment, 2018, 182: 263-274.
- [4] Gao M, Saide P E, Xin J Y, et al. Estimates of health impacts and radiative forcing in winter haze in eastern China through constraints of surface PM_{2.5} predictions [J]. Environmental Science & Technology, 2017, 51(4): 2178-2185.
- [5] Ma Y X, Zhao Y X, Yang S X, et al. Short-term effects of ambient air pollution on emergency room admissions due to cardiovascular causes in Beijing, China [J]. Environmental Pollution, 2017, 230: 974-980.
- [6] Ma Y X, Yang S X, Zhou J D, et al. Effect of ambient air pollution on emergency room admissions for respiratory diseases in Beijing, China[J]. Atmospheric Environment, 2018, 191: 320-327.
- [7] Wei Y, Li J, Wang Z F, et al. Trends of surface PM_{2.5} over Beijing-Tianjin-Hebei in 2013-2015 and their causes; emission controls vs. meteorological conditions [J]. Atmospheric and Oceanic Science Letters, 2017, 10(4): 276-283.
- [8] Chen Z H, Cheng S Y, Li J B, et al. Relationship between atmospheric pollution processes and synoptic pressure patterns in northern China[J]. Atmospheric Environment, 2008, 42 (24): 6078-6087.
- [9] Zhang Y, Ding A J, Mao H T, et al. Impact of synoptic weather patterns and inter-decadal climate variability on air quality in the North China Plain during 1980- 2013 [J]. Atmospheric Environment, 2016, 124: 119-128.
- [10] Liu Y Z, Wang B, Zhu Q Z, et al. Dominant synoptic patterns and their relationships with PM_{2, 5} pollution in winter over the Beijing-Tianjin-Hebei and Yangtze River delta regions in China [J]. Journal of Meteorological Research, 2019, 33 (4): 765-776
- [11] Wei P, Cheng S Y, Li J B, et al. Impact of boundary-layer anticyclonic weather system on regional air quality [J]. Atmospheric Environment, 2011, 45(14): 2453-2463.
- [12] Kang H Q, Zhu B, Gao J H, et al. Potential impacts of cold frontal passage on air quality over the Yangtze River Delta, China [J]. Atmospheric Chemistry and Physics, 2019, 19(6): 3673-3685.
- [13] Kang H Q, Zhu B, Su J F, et al. Analysis of a long-lasting haze episode in Nanjing, China [J]. Atmospheric Research, 2013, 120-121: 78-87.
- [14] Gao M, Carmichael G R, Wang Y, et al. Modeling study of the 2010 regional haze event in the North China Plain [J]. Atmospheric Chemistry and Physics, 2016, 16(3): 1673-1691.
- [15] Zhou S D, Peng S L, Wang M, et al. The characteristics and contributing factors of air pollution in Nanjing: A case study based on an unmanned aerial vehicle experiment and multiple datasets [J]. Atmosphere, 2018, 9 (9), doi: 10. 3390/atmos9090343.
- [16] Wang H, Xue M, Zhang X Y, et al. Mesoscale modeling study of the interactions between aerosols and PBL meteorology during a haze episode in Jing-Jin-Ji (China) and its nearby surrounding region-Part 1: Aerosol distributions and meteorological features [J]. Atmospheric Chemistry and Physics, 2015, 15(6): 3257-3275.

[17] Wang H, Shi G Y, Zhang X Y, et al. Mesoscale modelling study of the interactions between aerosols and PBL meteorology during a haze episode in China Jing-Jin-Ji and its near surrounding region-Part 2: Aerosols' radiative feedback effects [J]. Atmospheric Chemistry and Physics, 2015, 15(6): 3277-3287.

43 卷

- [18] 蒋永成. 海峡西岸地区大气复合污染变化和区域传输特征研究[D]. 南京:南京信息工程大学,2016.
- [19] Yu C, Zhao T L, Bai Y Q, et al. Heavy air pollution with a unique "non-stagnant" atmospheric boundary layer in the Yangtze River middle basin aggravated by regional transport of PM_{2.5} over China [J]. Atmospheric Chemistry and Physics, 2020, 20(12); 7217-7230.
- [20] 杨旭, 蔡子颖, 韩素芹, 等. 基于无人机探空和数值模拟天津一次重污染过程分析[J]. 环境科学, 2021, 42(1): 9-18. Yang X, Cai Z Y, Han S Q, et al. Heavy pollution episode in Tianjin based on UAV meteorological sounding and numerical model[J]. Environmental Science, 2021, 42(1): 9-18.
- [21] Huang X, Ding A J, Wang Z L, et al. Amplified transboundary transport of haze by aerosol-boundary layer interaction in China [J]. Nature Geoscience, 2020, 13(6): 428-434.
- [22] Liu Y B, Warner T T, Bowers J F, et al. The operational mesogamma-scale analysis and forecast system of the U. S. army test and evaluation command. Part I: Overview of the modeling system, the forecast products, and how the products are used [J]. Journal of Applied Meteorology and Climatology, 2008, 47 (4): 1077-1092.
- [23] Stauffer D R, Seaman N L. Use of four-dimensional data assimilation in a limited-area mesoscale model. Part 1; Experiments with synoptic-scale data [J]. Monthly weather review, 1990, 118(6): 1250-1277.
- [24] Janjié Z I. The step-mountain eta coordinate model: Further developments of the convection, viscous sublayer, and turbulence closure schemes[J]. Monthly weather review, 1994, 122(5): 927-945.
- [25] Emmons L K, Walters S, Hess P G, et al. Description and evaluation of the model for ozone and related chemical tracers, version 4 (MOZART-4)[J]. Geoscientific Model Development, 2010, 3(1): 43-67.
- [26] Guenther A, Karl T, Harley P, et al. Estimates of global terrestrial isoprene emissions using MEGAN (model of emissions of gases and aerosols from nature) [J]. Atmospheric Chemistry and Physics, 2006, 6(11): 3181-3210.
- [27] Kwok R H F, Fung J C H, Lau A K H, et al. Numerical study on seasonal variations of gaseous pollutants and particulate matters in Hong Kong and Pearl River Delta Region [J]. Journal of Geophysical Research: Atmospheres, 2010, 115, doi: 10. 1029/2009JD012809.
- [28] Boylan J W, Russell A G. PM and light extinction model performance metrics, goals, and criteria for three-dimensional air quality models [J]. Atmospheric Environment, 2006, 40 (26): 4946-4959.
- [29] 张晨,朱彬,刘晓慧,等.一次冷锋过程中我国区域空气污染边界层特征[J].中国环境科学,2020,40(10):4284-4291.
 - Zhang C, Zhu B, Liu X H, *et al.* Boundary layer characteristics of an air pollution event in China during a cold front [J]. China Environmental Science, 2020, **40**(10): 4284-4291.
- [30] Xu Y W, Zhu B, Shi S S, et al. Two inversion layers and their impacts on PM_{2.5} concentration over the Yangtze River Delta, China [J]. Journal of Applied Meteorology and Climatology, 2019, 58(11): 2349-2362.

HUANJING KEXUE

Environmental Science (monthly)

Vol. 43 No. 1 Jan. 15, 2022

CONTENTS

Characteristics and Risk Assessment of Heavy Metals in Urban Soils of Major Cities in China	PENG Chi, HE Ya-lei, GUO Zhao-hui, et al. (1)
Environmental Behaviors of Plant Growth Regulators in Soil: A Review Preparation and Application of Magnetic Water Treatment Materials Based on Iron Sludge	CHEN Liang, HOU Jie, HU Xiao-lei, et al. (11)
Preparation and Application of Magnetic Water Treatment Materials Based on Iron Sludge Meta-analysis of the Impact of Different Ozone Metrics on Total Mortality in China	RUAN Fang-fang, LIU Ji-xin, CHEN Zhi-wei, et al. (37)
Variation Characteristics and Potential Sources of the Mt. Haituo Aerosol Chemical Composition in Different Pollution Processes Duri	ing Winter in Beijing, China
Real-time Source Apportionment of PM _{2,5} and Potential Geographic Origins of Each Source During Winter in Wuhan	JIANG Shu-ning, KONG Shao-fei, ZHENG Huang, et al. (61)
Spatiotemporal Distribution and Seasonal Characteristics of Regional Transport of PM ₂ in Yuncheng City	· · · WANG Yun-tao ZHANG Oiang WEN Xiao-yu et al. (74)
Three-dimensional Structure Variation of PM _{2.5} During Cold Front Advance in Eastern China Pollution Characteristics and Risk Assessment of Nitrated Polycyclic Aromatic Hydrocarbons in the Atmosphere of Guangdong-Hong I	
	······ LI Yan-xi, XIE Dan-ping, LI Yu-ging, et al. (93)
Atmospheric VOCs Pollution Characteristics and Health Risk Assessment of Large-scale Integrated Industrial Area and Surrounding A	Areas in Southwest China
Characteristics and Source Apportionment of Ambient VOCs in Lhasa	·········· YU Jia-van HAN Yan CHEN Mu-lan et al. (113)
Variation Characteristics of Ambient Volatile Organic Compounds (VOCs) Volume Fraction During Hangzhou COVID-19 Period Role of Atmospheric VOCs in Ozone Formation in Summer in Shanghai Suburb	LIN Xu, YAN Ken-chang, JIN Jia-jia, et al. (123)
Characteristics of VOCs and Formation Potentials of O ₃ and SOA in Autumn and Winter in Tongchuan, China	········ YI Xiao-xiao, LI Jiang-hao, LI Guang-hua, et al. (140)
Emission Characteristics and Emission Factors of Volatile Organic Compounds from E-waste Dismantling and Recycling Processes	
Nonlinear Response Relationship Between Ozone and Precursor Emissions in the Pearl River Delta Region Under Different Transmiss	· WU Yong-kang, CHEN Wei-hua, YAN Feng-hua, et al. (160)
Characteristics of Ozone Pollution and Influencing Factors in Urban and Suburban Areas in Zibo	···· WANG Yu-van, YANG Wen, WANG Xiu-van, et al. (170)
Pollution Characteristics and Health Risk of Heavy Metals in Fugitive Dust Around Zhaotong City Characteristics of Microplastic Present in Urban Road Dust	PANG Xiao-chen, HAN Xin-yu, SHI Jian-wu, et al. (180)
Stable Isotopes of Precipitation in the Eastern Tarim River Basin and Water Vapor Sources	SONG Yang, WANG Sheng-ije, ZHANG Ming-iju, et al. (199)
Characteristics and Risk Assessment of Antibiotic Contamination in Chishui River Basin, Guizhou Province, China	WU Tian-yu, LI Jiang, YANG Ai-jiang, et al. (210)
Hydrochemical Characteristics and Controlling Factors of Surface Water and Groundwater in Wuding River Basin ————————————————————————————————————	LI Shu-jian, HAN Xiao, WANG Wen-hui, et al. (220)
rollution Characteristics and risk Assessment of Nutrients and fleavy metals in Sediments of the rune river influenced Area, Dailya	unggian lake CHEN Xing-hong, LI Li-qing, ZHANG Mei-vi, et al. (230)
Occurrence Characteristics of Microplastics in Mangrove Sediments in the Jiulong River Estuary and the Association with Heavy Meta	als ····· LIU Chang-jun, LUO Zhuan-xi, YAN Yu, et al. (239)
Quantitative Analysis of the Correlation Between Macrobenthos Community and Water Environmental Factors and Aquatic Ecosystem	Health Assessment in the North Canal River Basin of Beijing
Analysis on the Spatial Variability Mechanism of the Characteristic Water Quality Factors of Urban River Channel Reclaimed Water	LIU Quan-zhong, PENG Ke, SU Zhen-hua, et al. (256)
DOM Characteristics Analysis of Surface Sediment-overlying Water in Suzhou Landscape River Course	······ LI Chao-nan HE lie ZHU Xue-hui et al. (267)
Distribution of Typical Pollutants from Rainwater Sewer Sediments in Suzhou City Persistent Inhibition of Ammonium Released from Contaminated Sediments Through a Modified Zeolite and Biofilm System Enhanced	by Signaling Malagulas
Teisistein mindition of Annionium Released from Contaminated Sediments Through a modified Zeonie and Domini System Emanteed	XU Jin-lan, XU Yang, LI Xiu-min, et al. (285)
Effects of the Three Gorges Reservoir Operation on Vertical Distribution of Chlorophyll a and Environmental Factors in Tributaries	TIAN Pan, LI Ya-li, LI Ying-jie, et al. (295)
Characteristic Analysis of nirS Denitrifying Bacterial Community in Lijiahe Reservoir During Stratification	
Distribution Characteristics and Health Risk Assessment of Metal Elements for Groundwater in the Ningxia Region of China	······ WANG Xiao-dong, TIAN Wei, ZHANG Xue-yan (329)
Geochemical Characteristics and Driving Factors of High-Iodine Groundwater in Rapidly Urbanized Delta Areas; A Case Study of the	Pearl River Delta
Multimedia Distribution Characteristics and Risk Assessment of 22 PPCPs in the Water Environment of Oingru District Vangtza Riv	er Delta Demonstration Area
District Characteristics and the Assessment of 20 Paladacian J Paladacian Destruction of the Destruction of	·· ZHANG Zhi-bo, DUAN Yan-ping, SHEN Jia-hao, et al. (349)
Distribution Characteristics and Risk Assessment of 209 Polychlorinated Biphenyls in Dongting Lake and the Inflow Rivers Estimation of Nitrous Oxide Emission from River System Based on Water Discharge and Dissolved Nitrous Oxide Concentration	
Comparison Between Tributary and Main Stream and Preliminary Influence Mechanism of CO ₂ Flux Across Water-air Interface in Wa	anzhou in the Three Gorges Reservoir Area
Preparation of Functional Attapulgite Composite and Its Adsorption Behaviors for Congo Red	QIN Yu, OUYANG Chang-yue, WANG Yu-xiao, et al. (377)
Adsorption Characteristics and Long-term Effectiveness Evaluation of Iron-nitrogen Co-doped Biochar for Secondary Water-Soluble Or	rganic Matter WU Chen-xi, XU Lu, JIN Xin, et al. (398)
Nitritation Performance of Zeolite Moving Bed Biofilm Reactor for Ammonium Wastewater Treatment	······ DENG Cui-lan, GUO Lu, WANG Xiao-jun, et al. (409)
Effect of Temperature on ANAMMOX Process in Sequencing Batch Biofilm Reactors: Nitrogen Removal Performance and Bacterial C	Community
Effects of Carriers on ANAMMOX Sludge Activity Recovery and Microbial Flora Characteristics	······ LUO Jing-wen, YANG Jin-jin, LI Shao-kang, et al. (424)
Spatial Distribution and Source Analysis of Soil Heavy Metals in a Small Watershed in the Mountainous Area of Southern Ningxia Ba	sed on PMF Model
Heavy Metal Concentration Characteristics and Health Risks of Farmland Soils in Typical Pyrite Mining Area of the Central Zheijang	Province China
Did 7 . CH. Mali . D. L. A d. Dil C. I.D. L. D. L. A b. I.D. L.	····· CHENG Xiao-meng, SUN Bin-bin, WU Chao, et al. (442)
Risk Zoning of Heavy Metals in a Peri-urban Area in the Black Soil Farmland Based on Agricultural Products Main Control Factors of Cadmium Content in Rice in Carbonate Rock Region of Guangxi Based on the DGT Technique	
Inhibitory Effects of Soil Amendment Coupled with Water Management on the Accumulation of Cd and Pb in Double-Cropping Rice	······ LI Lin-feng, WANG Yan-hong, LI Yi-chun, et al. (472)
Characteristics and Health Risk Assessment of Cadmium, Lead, and Arsenic Accumulation in Leafy Vegetables Planted in a Greenh	OUSE CAO D.: CUN H 401
Pollution Characteristics and Health Risk Assessment of Polychlorinated Biphenyls in E-waste Disposal Residue-Soil-Vegetable	
Soil-crop Distribution and Health Risk Assessment of Organochlorine Pesticides on Typical Agricultural Land in Southern Leizhou Pe	ningula
Effects of Heavy Metal Content on Fungal Community Structure in Urban Soil	LIANG Xiao-hui, XIE Qi-lai, ZHENG Qian, et al. (500)
Effects of Long-term Fertilization on Soil Nutrient Characteristics and Microbial Resource Restrictions in a Terrace on the Loess Plate	egii
Effects of Eding term retinization on our values conductories and successful resolute resolutions in a retirect of the Edicard	·· WU Chun-xiao, GAO Xiao-feng, YAN Ben-shuai, et al. (521)
Microbial Composition and Diversity in Soil of Torreya grandis ev. Merrillii Relative to Different Cultivation Years After Land Use C	··· JIANG Ni-wen, LIANG Chen-fei, ZHANG Yong, et al. (530)
Effect of Combined Application of Biochar with Chemical Fertilizer and Organic Fertilizer on Soil Phosphatase Activity and Microbial	YANG Wen-na, YU Luo, LUO Dong-hai, et al. (540)
Extracellular Enzyme Stoichiometry and Microbial Metabolism Limitation During Vegetation Restoration Process in the Middle of the	Oinling Mountains China
Effects of Biodegradable Film Raw Material Particles on Soil Properties, Wheat Growth, and Nutrient Absorption and Transportation	
Effects of Stalk Incorporation on Soil Carbon Sequestration, Nitrous Oxide Emissions, and Global Warming Potential of a Winter Wh	neat-Summer Maize Field in Guanzhong Plain
Enects of state incorporation of soil carbon expectation, virtual state energial and of soil and provide the virtual state of the soil carbon expectation, virtual state energy and of the soil carbon energy and of the	··· WAN Xiao-nan, ZHAO Ke-yue, WU Xiong-wei, et al. (569)